

1           **Quantifying inclination shallowing and representing**  
2           **flattening uncertainty in sedimentary paleomagnetic**  
3           **poles**

4           **James Pierce<sup>1,2</sup>, Yiming Zhang<sup>1</sup>, Eben B. Hodgin<sup>1</sup>, Nicholas L.**  
5           **Swanson-Hysell<sup>1</sup>**

6           <sup>1</sup>Department of Earth and Planetary Science, University of California, Berkeley, CA, USA

7           <sup>2</sup>Department of Earth and Planetary Sciences, Yale University, New Haven, CT, USA

8           **Key Points:**

- 9           • Inclination shallowing is empirically quantified in 1.1 Ga clastic sedimentary rocks  
10          bracketed by volcanics
- 11          • Detrital hematite remanence is flattened by a factor of  $0.61_{0.55}^{0.67}$  relative to unflat-  
12          tened pigmentary hematite
- 13          • Flattening factor uncertainty is present in all methods and should be incorporated  
14          into the uncertainty of sedimentary paleomagnetic poles

---

Corresponding author: James Pierce (james.pierce@yale.edu); Nicholas Swanson-Hysell  
(swanson-hysell@berkeley.edu),

15 **Abstract**

Inclination is the angle of a magnetization vector from horizontal. Clastic sedimentary rocks often experience inclination shallowing whereby syn- to post-depositional processes result in flattened detrital remanent magnetizations relative to local geomagnetic field inclinations. The deviation of recorded inclinations from the true values presents challenges for reconstructing paleolatitudes. A widespread approach for estimating the flattening factor ( $f$ ) compares the shape of an assemblage of magnetization vectors to that derived from a paleosecular variation model (the elongation/inclination [ $E/I$ ] method). However, few studies exist that compare the results of this statistical approach with empirically determined flattening factors and none in the Proterozoic Eon. In this study, we evaluate inclination shallowing within 1.1 billion-year-old, hematite-bearing, inter-flow red beds of the Cut Face Creek Sandstone that is bounded by lava flows of known inclination. We found that detrital hematite remanence is flattened with  $f = 0.65_{0.56}^{0.75}$  whereas the pigmentary hematite magnetization shares a common mean with the volcanics. Comparison of detrital and pigmentary hematite directions results in  $f = 0.61_{0.55}^{0.67}$ . These empirically determined flattening factors are consistent with those estimated through the  $E/I$  method ( $f = 0.64_{0.51}^{0.85}$ ) supporting its application in deep time. However, all methods have significant uncertainty associated with determining the flattening factor. This uncertainty can be incorporated into the calculation of paleomagnetic poles with the resulting ellipse approximated with a Kent distribution. Rather than seeking to find “the flattening factor,” or assuming a single value, the inherent uncertainty in flattening factors should be recognized and incorporated into paleomagnetic syntheses.

37 **Plain Language Summary**

The magnetization of ancient sedimentary rocks provides great insight into Earth's past. Earth scientists use these rocks to understand how Earth's magnetic field has flipped through time and to reconstruct how continents have moved. Hematite is a common mineral which gives many sandstones a red color — leading geologists to refer to them as “red beds.” While hematite is a reliable magnet through time, the magnetic directions recorded by hematite grains can be shallower than the geomagnetic field (i.e. they are flattened). Magnetization steepness is how Earth scientists determine the latitude where rocks were deposited as the magnetic field gets steeper towards the pole. We need ways to correct for magnetization shallowing in sedimentary rocks. In this study, we compared

47 the steepness of magnetic directions held by hematite to that of lava flows that formed  
 48 in the same time interval. Magnetic directions from lava flows are not flattened so this  
 49 comparison allows us to determine the shallowing amount. We compare it to a statisti-  
 50 cal method and see that the results are indistinguishable within the appreciable un-  
 51 certainty of the methods. Earth scientists should include the uncertainty associated with  
 52 inclination shallowing when they report ancient pole positions determined from such flat-  
 53 tened magnetic directions.

## 54 1 Introduction

Hematite-bearing sedimentary rocks at Earth's surface are widespread and serve as an important paleomagnetic recorder. The geocentric axial dipole (GAD) hypothesis posits that the long-term average of Earth's magnetic field is dipolar and that the time-averaged geomagnetic pole overlaps with the geographic pole. Using this hypothesis, the inclination ( $I$ ) of a rock's magnetization can be translated into an interpreted paleolatitude ( $\phi$ ) of the location where the rock formed using the dipole formula:

$$\tan(I) = 2 \tan(\phi)$$

55 Unfortunately, the accuracy of paleomagnetic directions recorded by the detrital rema-  
 56 nent magnetization (DRM) of sedimentary rocks has long been recognized as problem-  
 57 atic due to the issue of inclination shallowing (King, 1955; Tauxe & Kent, 1984; Kodama,  
 58 2012). The rotation of ferromagnetic grains during deposition and compaction can re-  
 59 sult in the acquisition of a detrital remanent magnetization that is biased shallow rel-  
 60 ative to the local geomagnetic field in which it was acquired (Tauxe, 2005). If uncorrected,  
 61 shallower inclinations obtained from sedimentary rocks can potentially result in erroneously  
 62 low estimates of paleolatitudes, biasing the interpreted past positions of continents and  
 63 hindering plate reconstructions (Domeier et al., 2012). Despite this challenge, the abun-  
 64 dance and long-term magnetic and geochemical stability of hematite makes hematite-  
 65 bearing sedimentary rocks a very important archive of Earth history.

66 In addition to detrital hematite grains that can carry a DRM, hematite-bearing  
 67 sedimentary rocks often have a distinct population of pigmentary hematite that give "red  
 68 beds" their characteristic red color. This finer-grained pigmentary hematite precipitates  
 69 following deposition and carries a chemical remanent magnetization (CRM) acquired dur-  
 70 ing crystal growth (Tauxe et al., 1980; Jiang et al., 2015; Swanson-Hysell et al., 2019).

This pigmentary hematite can form from metastable Fe(III) oxide precursors such as ferrihydrite (Gutiérrez et al., 2016; Jiang et al., 2018, 2022). Such pigmentary hematite records a magnetization when it grows to be the size of a stable single domain particle ( $\sim 30$  nm; Özdemir and Dunlop (2014)). Although the CRMs acquired by pigmentary hematite are not expected to be shallowed, the time lag between sediment deposition and secondary pigmentary hematite formation can be variable which complicates interpretations. Fortunately, magnetization held by primary detrital hematite can be isolated from that held by finer-grained secondary pigmentary hematite through high resolution thermal demagnetization as hematite grains less than  $\sim 400$  nm in diameter will unblock at lower temperatures than coarser detrital grains (Tauxe et al., 1980; Swanson-Hysell et al., 2019). After thermal demagnetization of pigmentary hematite, the DRM held by coarser hematite grains will become apparent near hematite's Néel Temperature ( $\sim 682^\circ\text{C}$ ; Butler (1992); Lu and Meng (2010)).

To elucidate factors that contribute to inclination shallowing of detrital magnetization in sedimentary rocks, King (1955) conducted laboratory redeposition experiments and quantified the shallowing effect with the flattening function:

$$\tan(I_o) = f \tan(I_f)$$

where  $I_o$  represents the observed inclination of the specimen magnetization and  $I_f$  represents the inclination of the field in which the magnetization was acquired (Fig. 1). The flattening factor  $f$  ranges from 1 for no flattening to 0 for completely flattened inclinations (Fig. 1). Further laboratory redeposition experiments have found that major contributing processes to inclination shallowing include the initial settling and deposition of particles as well as compaction during burial (Anson & Kodama, 1987; Tauxe & Kent, 1984; Sun & Kodama, 1992; Tan et al., 2002). The degree of flattening can also be influenced by sedimentary lithology with finer grained sediments exhibiting more inclination shallowing in laboratory experiments (Tan et al., 2002).

Correcting the effects of inclination shallowing is crucial for estimating the inclination of the geomagnetic field at the time of deposition. Two main classes of correction methods have been developed and applied in order to determine and correct for inclination shallowing. The first class of methods involves investigating the magnetic fabrics of the sedimentary rocks of interest. Such an approach was pioneered by Jackson et al. (1991), where anisotropy of anhysteretic magnetization (AARM) was used to es-

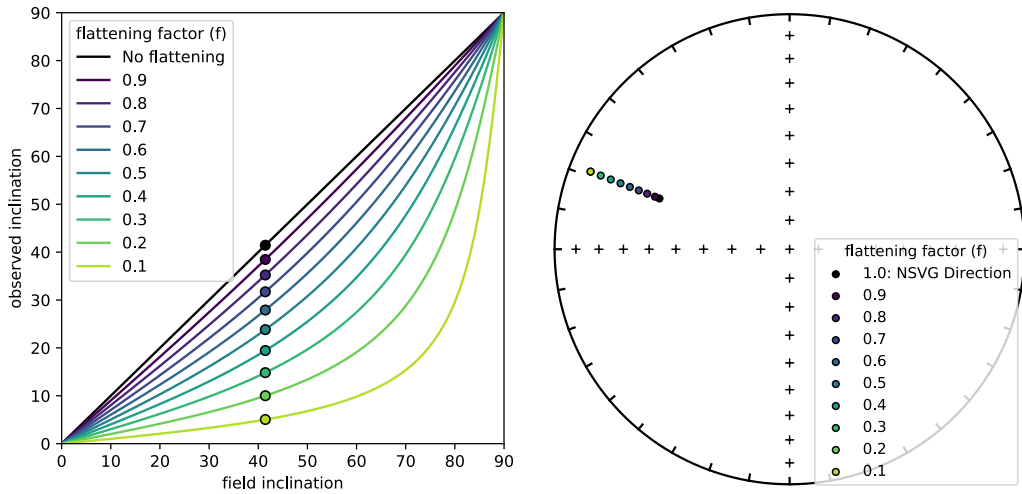


Figure 1: Left panel: the relationship between the inclination of the local magnetic field compared to the observed inclination of sedimentary rocks is shown for different flattening factors ( $f$ ). A value of 1.0 corresponds to no flattening while a value of 0.0 means the magnetizations are completely flattened. The dots show the inclination expected for the Cut Face Creek Sandstone that would result from variable flattening of the mean inclination of lavas from the upper northeast sequence of the North Shore Volcanic Group (NSVG; Tauxe and Kodama (2009); Swanson-Hysell et al. (2019)). Right panel: an equal area plot with the mean paleomagnetic direction of the upper northeast sequence North Shore Volcanic Group lavas (declination of 290.7°; inclination of 41.4°) and the directions that would result from applying different flattening factors.

99 estimate and correct shallowed inclinations. Subsequent work has highlighted the importance  
 100 of determining the relationship between shallowing and magnetic anisotropy as-  
 101 sociated with a given sedimentary rock in the application of the method (Kodama, 2012).  
 102 A particular difficulty in applying this method to correct detrital remanent magnetiza-  
 103 tions in hematite-bearing sedimentary rocks is that both pigmentary hematite and de-  
 104 trital hematite contribute to the overall magnetic fabric with the anisotropy associated  
 105 with the detrital population needing to be isolated for an inclination shallowing correc-  
 106 tion. Recognizing this challenge, Bilardello (2015) developed a more involved multispec-  
 107 imen approach using step-wise thermal demagnetization of applied isothermal remanent  
 108 magnetizations (IRM) in order to isolate the anisotropy of DRM. Overall, such anisotropy  
 109 approaches are labor-intensive and have only been applied to quantify inclination shal-  
 110 lowing in a modest number of studies.

111 The other principal method for correcting inclination shallowing is the statistical  
 112 elongation/inclination ( $E/I$ ) approach (Tauxe & Kent, 2004). This method utilizes the  
 113 fact that inclination shallowing will skew the shape of the population of recorded mag-

netization vectors away from a distribution expected from secular variation of Earth's magnetic field. The  $E/I$  method uses the TK03 model for paleosecular variation which is based on a compilation of paleomagnetic directions from lava flows of the last 5 million years (McElhinny & McFadden, 1997) to predict the original distribution and shape of paleomagnetic directions based on a Giant Gaussian Process approach. In this model, the distribution of paleomagnetic directions at a given latitude that sufficiently samples paleosecular variation has a predictable elongated shape that deviates from circular symmetry as a function of inclination. The shape of the distribution of vectors is quantified by the elongation parameter ( $E$ ) that can be determined by calculating the eigenvalue ratio  $\tau_2/\tau_3$  of the orientation matrix for a population of vectors. One can estimate the amount of inclination shallowing in a sedimentary rock by progressively unflattening the shallowed magnetization vectors until their distribution best matches the predicted shape. This approach assumes that the TK03.GAD model accurately characterizes the paleosecular variation during acquisition of magnetization in the sedimentary formation of interest. The uncertainty on the flattening factor that leads to a correspondence between the elongation of the magnetization vectors with the  $E/I$  of the TK03.GAD model can be estimated through bootstrap resampling (Tauxe & Kent, 2004). As a statistical method, the  $E/I$  has the benefit that the analyses are done on specimen DRM magnetization directions and it does not require additional labor-intensive anisotropy measurements which includes the necessary determination of individual particle anisotropy. However, this method requires a large number of DRM directions ( $>100$ ) as many more vectors are needed to accurately determine the shape of a distribution than the mean of a distribution (Tauxe et al., 2008). The large number of directions needed to reliably apply the method led Vaes et al. (2021) to propose a classification scheme wherein  $>100$  directions are needed for a corrected sedimentary pole to be deemed reliable (as well as paleosecular variation being assessed using the criteria of Deenen et al. (2011)).

Due to the challenges of applying these inclination correction methods, particularly to previously published data, another simplified approach that has been taken in the literature is to assume an average  $f$  factor and apply it to the mean direction calculated from a sedimentary rock (Domeier et al., 2012; Torsvik et al., 2012). For many published data sets from sedimentary rocks where the specimen level data are not available and compilations are reliant on study level means, such an approach is the only one that can be applied without redoing the study. This approach was applied by Torsvik et al. (2012)

in their compilation of Phanerozoic paleomagnetic poles where a flattening factor of 0.6 was used to correct sedimentary poles. Domeier et al. (2012) also adopted a flattening factor of 0.6 acknowledging that to do so is an oversimplification, but a value that is consistent with compiled  $f$  factor estimates (such as those of Bilardello and Kodama (2010c)). This approach has been criticized as disregarding the variability of  $f$  factors that can result from differences in lithology and magnetic carriers (Bilardello, 2016; Vaes et al., 2021). There have been other novel data analysis approaches to seek to constrain  $f$  factors such as through comparing intersecting great circles from multiple paleomagnetic poles in the true dipole pole method of Gallo et al. (2017). For any method, there is a challenge of applying a single  $f$  factor to a sedimentary formation given variability associated with grain size and other conditions.

In this study, we use the ca. 1093 Ma Cut Face Creek Sandstone to empirically constrain the magnitude of inclination shallowing. The Cut Face Creek Sandstone is a ~95 meter-thick interval of interflow red siltstone and sandstone deposited in a fluvial overbank depositional environment between lava flows of the upper northeast sequence of the North Shore Volcanic Group (Fig. 2). Since the sandstone is bracketed by lava flows with known age and existing paleomagnetic data, its age and expected paleomagnetic direction is well constrained (Tauxe & Kodama, 2009; Swanson-Hysell et al., 2019). We compare the detrital remanence directions of the Cut Face Creek specimens to the expected directions from the volcanics to determine the amount of inclination shallowing that took place within the sedimentary unit. Next, we apply the elongation/inclination method to the isolated DRM directions to obtain statistical estimates for the amount of shallowing that can be compared to the empirically determined value. Finally, we present recommendations for the incorporation of uncertainties in flattening factor estimates into sedimentary paleomagnetic poles and paleolatitude estimates as such uncertainties are present regardless of the method through which they are determined.

## 2 Geologic Setting and stratigraphy of the Cut Face Creek Sandstone

The Mesoproterozoic Midcontinent Rift is a protracted intracontinental rift punctuated by rapid and voluminous magmatism throughout its history (Fig. 2A; Green (1983); Swanson-Hysell et al. (2021)). A ~8 km thick succession of lava flows that erupted during Midcontinent Rift development is exposed in northeastern Minnesota forming the northeast sequence of the North Shore Volcanic Group (Fig. 2B; Green et al. (2011)).

Our study is focused on the ~95-meter-thick Cut Face Creek Sandstone which is an interflow fluvial siliciclastic unit that was deposited during a hiatus in lava flow eruptions (Jirsa, 1984). It is bracketed by the underlying Good Harbor Bay andesites and the overlying Terrace Point Basalt (Figs. 2C and 3). These units are all part of the normal-polarity upper northeast sequence of the North Shore Volcanic Group (Figs. 2; Green et al. (2011)). The Grand Marais Rhyolite with a high-precision weighted mean  $^{206}\text{Pb}/^{238}\text{U}$  zircon date of  $1093.52 \pm 0.43$  Ma (Swanson-Hysell et al., 2019) is ~250 m stratigraphically below the Good Harbor Bay andesites (Green et al., 2011). Its age serves as a maximum age constraint for the deposition of Cut Face Creek Sandstone and is likely close to the absolute age. The minimum depositional age of the sandstone is constrained by the  $1091.7 \pm 0.2$  Ma Beaver River diabase of the Beaver Bay Complex, which crosscuts the North Shore Volcanic Group (Zhang et al., 2021). Paleomagnetic data from twenty-eight lava flows of the upper Northeast sequence of the North Shore Volcanic Group (blue diamonds in Fig. 2; Books (1972); Tauxe and Kodama (2009)) result in a paleomagnetic pole at  $181.7^\circ\text{E}$ ,  $31.1^\circ\text{N}$  ( $A_{95}=4.2^\circ$ ; Swanson-Hysell et al. (2019)). This pole from the volcanics can be used to calculate an expected paleomagnetic direction for the Cut Face Creek Sandstone with a declination of  $290.7^\circ$  and an inclination of  $41.4^\circ$  (Fig. 1).

The Cut Face Creek Sandstone is well-exposed in a prominent roadcut along Minnesota State Highway 61 with a striking deep red color ( $47.7280^\circ\text{N}$ ,  $90.4428^\circ\text{W}$ ; Figs. 2 and 3). Throughout the section, the strata are consistently tilted to the southeast with an average dip direction of  $166.5^\circ$  and dip of  $10.0^\circ$  (based on 44 measurements). Our stratigraphic section through the ~95-meter-thick Cut Face Creek Sandstone was measured at a decimeter scale upward from its base where it overlies the uppermost lava flow of the Good Harbor Bay andesites (Fig. 3).

The Good Harbor Bay andesites are fine-grained, greenish-grey, volcanic rocks that become increasingly vesicular toward flow tops. In the measured stratigraphic section, the uppermost lava is overlain by a 0.9-meter-thick silt-sized matrix-supported basalt pebble conglomerate with sand lenses and mud cracks (Fig. 3). This conglomerate is followed by ~17.5 m of medium to fine-grained lithic arkose that generally fines upwards. The medium-grained sandstone is associated with occasional decimeter-scale dune-scale trough cross-bedding characteristic of channel bars. Finer-grained sandstone beds that contain regular mm-scale siltstone laminae, mudcracks, and current ripples with variable flow directions, are characteristic of crevasse splay deposits which occur when a stream

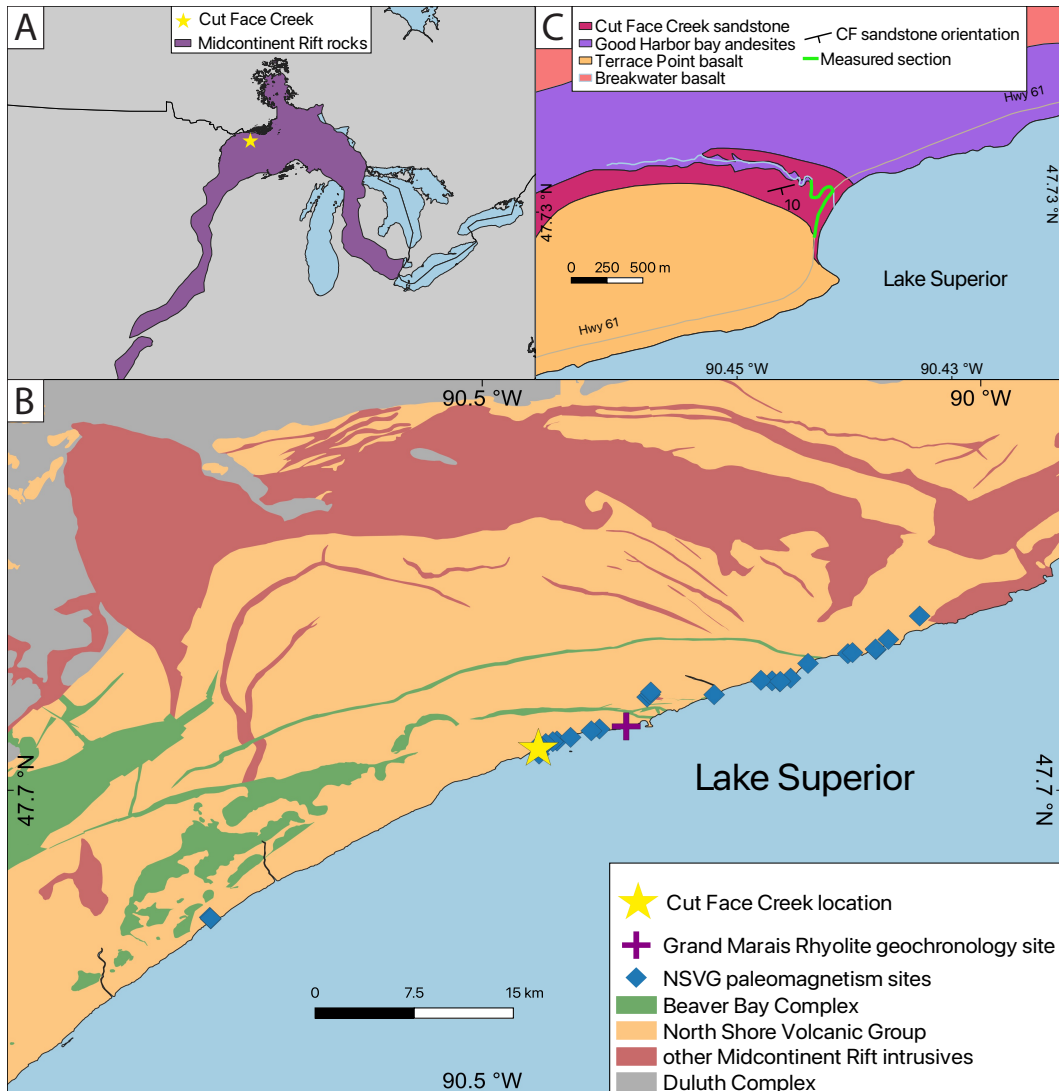


Figure 2: A) Overview map showing the location of the Cut Face Creek Sandstone (yellow star;  $47.7280^{\circ}\text{N}$ ,  $90.4428^{\circ}\text{W}$ ) within the extent of the Midcontinent Rift. B) Geologic map along the North Shore of Lake Superior showing the location of the Cut Face Creek Sandstone (yellow star) within the upper northeast sequence of the North Shore Volcanic Group (NSVG; geologic data from Miller et al. (2001)). CA-ID-TIMS  $^{206}\text{Pb}/^{238}\text{U}$  dates constrain the Cut Face Creek Sandstone to be younger than the  $1093.52 \pm 0.43$  Ma Grand Marais Rhyolite (purple cross; Swanson-Hysell et al. (2019)) and older than the  $1091.7 \pm 0.2$  Ma cross-cutting Beaver River diabase of the Beaver Bay Complex (green unit, Zhang et al. (2021)). C) The Cut Face Creek Sandstone overlies the Good Harbor Bay andesite (purple) while the Terrace Point basalt (tan orange) erupted atop the sandstone. The green line indicates the location of the measured stratigraphic section shown in Fig. 3.

212 overflows its channel leading to overbank deposition (e.g. van Toorenenburg et al., 2018).  
 213 The next  $\sim 11.8$  m of strata continue to fine upwards and are dominated by very fine to  
 214 fine-grained sandstone containing interbeds of cm-scale siltstone. This interval, which  
 215 contains siltstone rip-up clasts and current ripples with variable flow directions (Fig. 3),

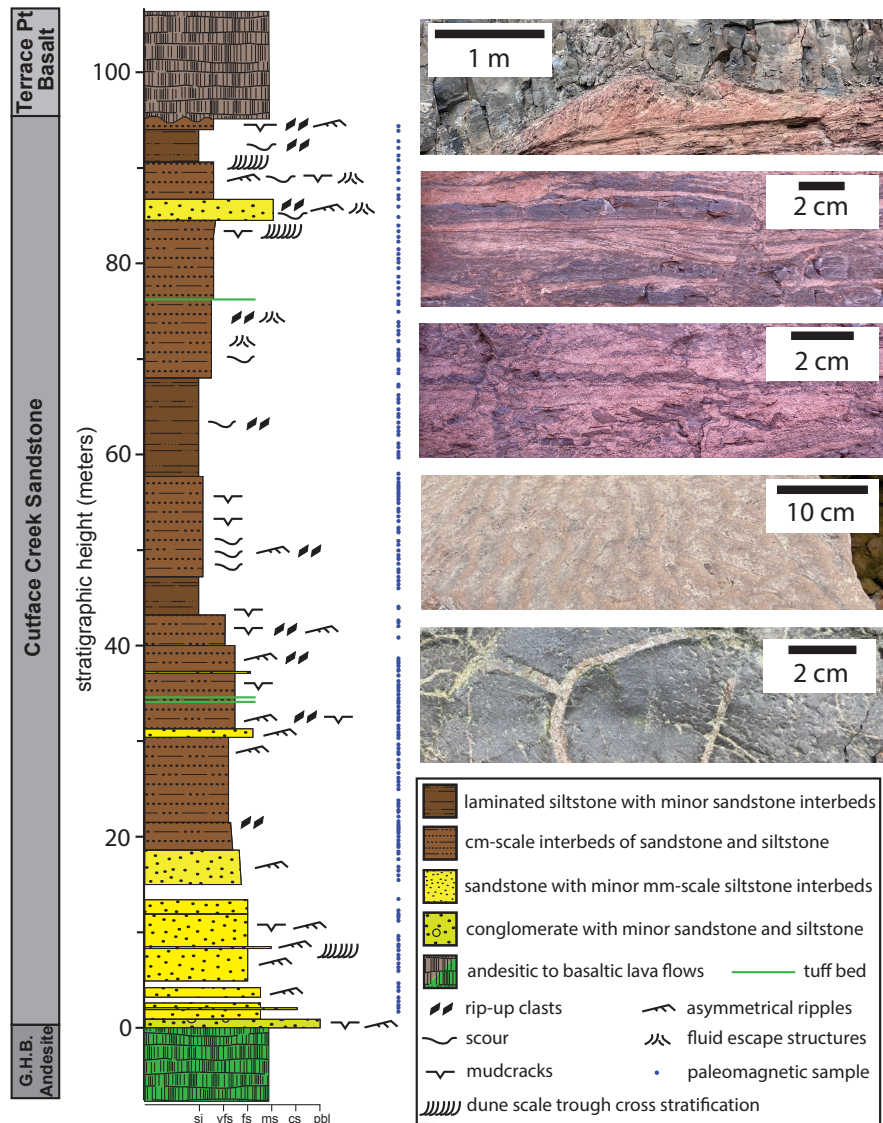


Figure 3: Stratigraphic column of the 95-meter-thick Cut Face Creek Sandstone as exposed along Cut Face Creek and Hwy 61 (Fig. 2). The Cut Face Creek Sandstone was deposited during a hiatus in eruption of the lavas North Shore Volcanic Group such that it is bracketed by the Good Harbor Bay andesites (G.H.B.; green) and the Terrace Creek Basalt (grey). Photos from bottom to top: top view of a mud-cracked siltstone layer within the basal conglomerate; oblique top view of current ripples in sandstone; side view of sandstone (light red) with tabular rip-up clasts of siltstone (dark red); side view of finely interbedded siltstone (dark red) and sandstone (light red) with asymmetric scour and ripple cross-stratification with fluid escape structures; upper contact with Terrace Point Basalt whose advance led to soft sediment deformation in the underlying Cut Face Creek Sandstone.

is characteristic of continued aggradation of crevasse splay deposits situated farther from the fluvial channel than the underlying interval. At 30.4 m, the stratigraphic trend is disrupted by a similar fining-upwards interval with a basal 1.1 m layer of medium-grained sandstone containing current ripples grading up into ~11.7 m of fine to very fine-grained

sandstone with regular interbeds of cm-scale siltstone, which by the top of the interval  
 are subequal in thickness. This interval contains cream-colored ash beds, mudcracks, cur-  
 rent ripples, and siltstone rip-up clasts consistent with an increasingly distal overbank  
 environment. The overlying ~41.3 m of strata is dominated by laminated siltstone, and  
 contains regular occurrences of mudcracks and siltstone rip-up clasts—consistent with  
 floodplain sedimentation. Within this interval, fine-grained sandstone is deposited in cm-  
 scale sheets characteristic of distal crevasse splay flooding events and in decimeter-scale  
 asymmetric scours characteristic of meandering channels within a floodplain (Cant & Walker,  
 1976), with the latter occasionally infilled by dune-scale trough cross-bedding. The up-  
 per ~15 m of the siltstone-dominated interval, coarsens upwards, and contains strata that  
 can be disrupted by dewatering structures and infilled cracks that may be attributed to  
 a combination of desiccation, shrinkage, and compaction (Fig. 3). The upper ~10.6 m  
 of the stratigraphic section coarsens upwards from ~30% siltstone to well-lithified fine-  
 to medium-grained sandstone, which was likely deposited in a crevasse splay environ-  
 ment in proximity to a fluvial channel. Flame structures associated with dewatering are  
 common throughout the top part of the section (Fig. 3) with some ripple-scale cross-bedding.  
 The uppermost 5 m include light tan colored horizons (Fig. 3) associated with fluid flow  
 and reduction of the pigmentary hematite. The top 1.1 m beneath the Terrace Point basalt  
 consists of baked siltstone with mudcracks and slaty cleavage. Eruption of the overly-  
 ing lava flow of the Terrace Point basalt folded and deformed the uppermost sediment  
 layers as it advanced and “bulldozed” the unconsolidated sediment (Fig 3).

Overall, these observations and interpretations are consistent with those of Jirsa  
 (1984) and Mitchell and Sheldon (2009) who invoke a fluvial depositional environment  
 dominated by overbank deposition. Flow in this fluvial system was dominantly to the  
 SSW with the composition of sandstone consistent with a provenance largely derived from  
 the local North Shore Volcanic Group (Jirsa, 1984).

### 3 Methods

Paleomagnetic cores from the Cut Face Creek Sandstone were sampled through the  
 strata with an interval of ~50 cm (Fig. 3). In order to maximize sampling of paleosec-  
 ular variation, we optimized for vertical stratigraphic coverage and collected one sam-  
 ple at each horizon. As such, each sample constitutes a paleomagnetic site considering  
 that a paleomagnetic site (which ideally captures a single snapshot of the local geomag-

netic field) is a particular bed in a sedimentary sequence. Dark red fine-grained siltstone layers were preferentially sampled as they have lower permeability and are less susceptible to diagenetic alteration through fluid flow than coarser grained sandstone. Care was taken to avoid samples containing reoriented siltstone rip-up clasts from underlying strata. Paleomagnetic samples were oriented using a magnetic compass and a sun compass whenever possible. Sun compass data were preferentially used when available.

The specimens underwent step-wise thermal demagnetization in the UC Berkeley Paleomagnetism Lab using an ASC demagnetizer (residual fields <10 nT) with measurements of remanent magnetization made on a 2G DC-SQUID magnetometer. The demagnetization protocol had increasingly high-resolution steps (5 to 2°C) approaching the Néel temperature of hematite (up to ~687°C). Implementing these high-resolution thermal demagnetization steps allowed us to isolate magnetic remanence components carried by coarser detrital hematite grains from finer pigmentary hematite grains (Fig. 4; Swanson-Hysell et al. (2019)). Least-squares fits were made to distinct components (Kirschvink, 1980) using PmagPy (Tauxe et al., 2016). All paleomagnetic data are available to the measurement level in the MagIC database (<https://earthref.org/MagIC/19603/789b4868-fb73-4315-af37-81f599cacc4a>; this link is for review purposes and will be updated when the manuscript is given a doi).

## 4 Results and Interpretation

### 4.1 Thermal demagnetization

High-resolution thermal demagnetization on the Cut Face Sandstone reveals three magnetization components: a low-temperature component that typically unblocks up to 200°C, a mid-temperature component that was typically removed up to 650°C, and a high-temperature component that was typically removed between 650°C and 687°C (Fig. 4). In the specimen demagnetization data, there is typically a shallowing of inclination from the mid-temperature component to the high-temperature component (Fig. 4). The high unblocking temperature range for the high temperature component is consistent with the interpretation that it is held by hematite grains that have sizes >400 nm and have unblocking temperatures close to the Néel temperature of hematite (Jiang et al., 2015; Swanson-Hysell et al., 2019). We interpret the high-temperature component to be a detrital remanent magnetization (DRM) acquired at the time of Cut Face Creek Sandstone

283 deposition. In contrast, the relatively lower unblocking temperatures and generally steeper  
 284 inclinations for the mid-temperature component is consistent with them being carried  
 285 by pigmentary hematite grains of smaller sizes (<400 nm) that record a chemical rema-  
 286 nent magnetization (CRM) during their growth within the sediment soon after deposi-  
 287 tion (Swanson-Hysell et al., 2019). Of the 179 samples analyzed from the Cut Face Creek  
 288 Sandstone, a high-temperature component was resolved in 157 specimens, while a mid-  
 289 temperature component was resolved in 167 specimens, and a low-temperature compo-  
 290 nent in 109 specimens (Fig. 4).

291 Fisher statistics were calculated to obtain mean directions for each component. In  
 292 geographic coordinates not corrected for bedding tilt, the mean low-temperature com-  
 293 ponent has a declination of 359.3° and an inclination of 67.2° ( $\alpha_{95}=2.0$ ;  $k=46.0$ ;  $n=109$ ;  
 294 Fig. 4). This direction is indistinguishable from the local expected dipole field (dec=000.0°,  
 295 inc=65.6°) consistent with it being a recently acquired viscous remanent magnetization.  
 296 The bedding tilt-corrected mid-temperature component has a mean declination of 286.5°  
 297 and an inclination of 42.0° ( $\alpha_{95}=1.6$ ;  $k=48.2$ ;  $n=167$ ). This direction is indistin-  
 298 guishable from the mean direction of the lava flows of the upper northeast sequence of the North  
 299 Shore Volcanic Group (dec=290.7°; inc=41.4°  $\alpha_{95}=4.9$ ;  $n=28$ ; Swanson-Hysell et al. (2019);  
 300 Fig. 5) as they pass a statistical common mean test. This directional similarity is con-  
 301 sistent with the interpretation that the pigmentary hematite grains within the Cut Face  
 302 Creek Sandstone formed soon after deposition as a CRM and did not experience shal-  
 303 lowing following formation. The tilt-corrected high-temperature component has a mean  
 304 declination of 286.6° and an inclination of 29.4° ( $\alpha_{95}=1.9$ ;  $k=35.8$ ;  $n=157$ ). The high-  
 305 temperature component has a nearly identical mean declination with that of the mid-  
 306 temperature component, but its mean inclination is shallower than that of the mid-temperature  
 307 component and that of the lava flows (Fig. 5). In addition to a shallower mean inclina-  
 308 tion, the shape of the distribution is skewed such that directions are more elongate to-  
 309 wards the horizontal plane consistent with sedimentary inclination flattening (Tauxe and  
 310 Kent (2004); resulting in an elongation axis trending NE-SW for this data set; Fig. 4).  
 311 This elongation contrasts with that of the mid-temperature component which is elon-  
 312 gate in the vertical plane (an elongation axis trending NW-SE for this data set) as ex-  
 313 pected for an unflattened distribution of directions (Fig. 4). Taken together with the un-  
 314 blocking temperatures consistent with detrital hematite, the shallowed inclination and

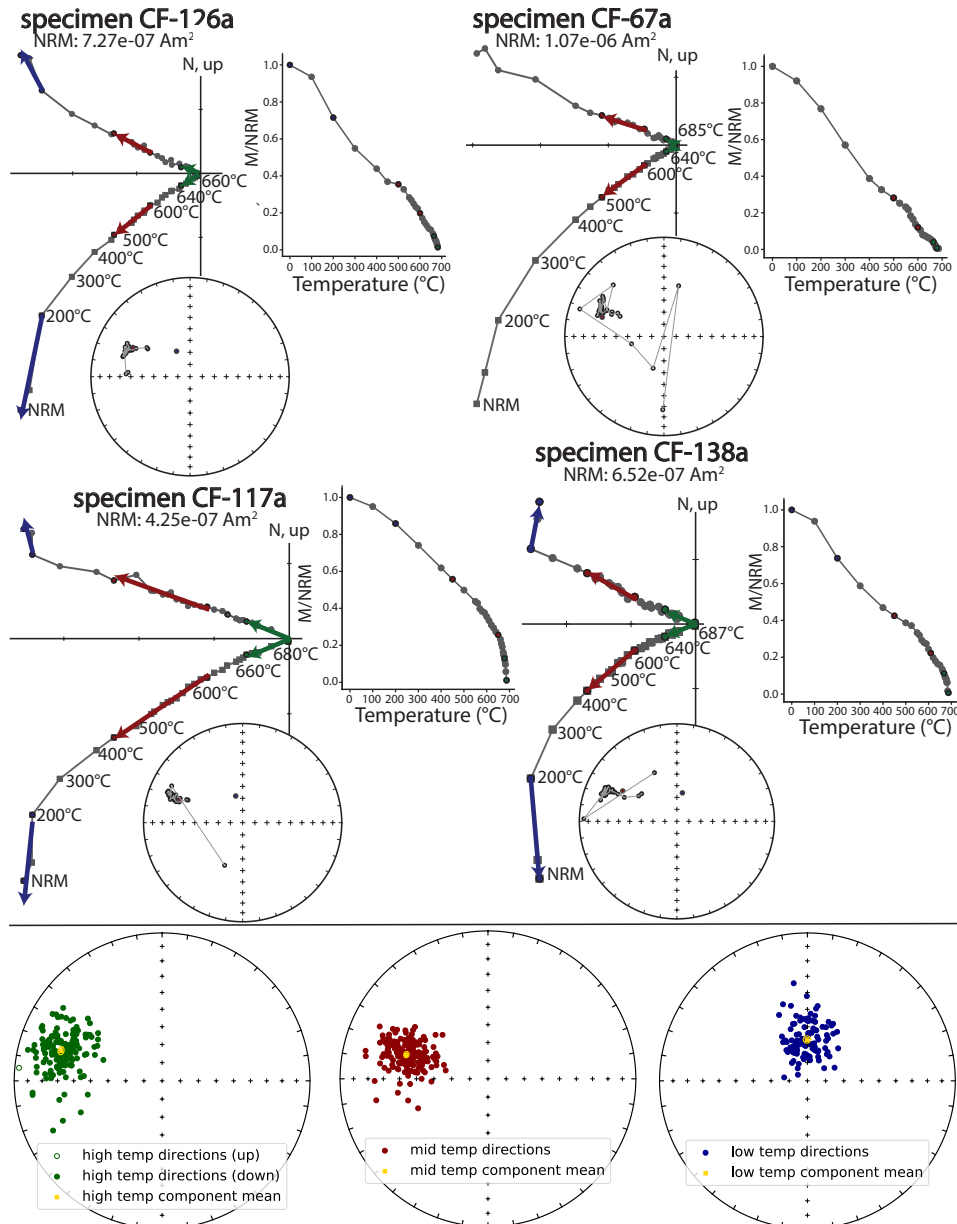


Figure 4: Example specimen thermal demagnetization results (top panel) and summary of all remanence components on equal area plots (bottom panel). The vector orthogonal plots show progressive magnetization direction changes through high-resolution demagnetization. The low-temperature component (blue) with a northerly declination and steep downward inclination is interpreted to have been acquired recently as its direction is indistinguishable from the present local axial dipole field. The mid-temperature component (red) is interpreted to be a chemical remanent magnetization (CRM) acquired soon after deposition of the Cut Face Creek Sandstone and was not flattened. The high temperature component (green) is interpreted as a detrital remanent magnetization (DRM) acquired through sediment deposition that was shallowed due to depositional and post-depositional processes.

the distribution shape indicate that the high-temperature magnetization is a detrital remanent magnetization.

317       **4.2 Empirical inclination shallowing assessment**

318       Given that the true paleomagnetic direction at the time of Cut Face Creek Sand-  
 319       stone deposition can be constrained by the records of the bracketing North Shore Vol-  
 320       canic Group and the sandstone's CRM directions which are not shallowed (i.e. they share  
 321       a common mean with the volcanic directions; Fig. 5A), we can empirically determine  
 322       the degree of inclination shallowing of the DRM and compare the results with that from  
 323       the statistical *E/I* method (Tauxe & Kent, 2004).

324       Given that there are uncertainties associated with each mean direction, there will  
 325       be a range of *f* factors that will steepen the DRM direction to share a common mean  
 326       with the directions that are not shallowed. To determine this range, we incrementally  
 327       corrected all specimen DRM directions by an *f* factor ranging from 1 to 0 with a step  
 328       size of 0.001 (Fig. 5). As *f* decreases from 1 to 0 (i.e. the amount of unflattening increases),  
 329       it is observed that the angles between the mean direction of the corrected DRM direc-  
 330       tions and those of both the CRM directions and the lava flow directions decrease toward  
 331       a minimum when *f* is around 0.6, which is followed by an increase as the directions are  
 332       steepened toward vertical (Fig. 5). In addition to calculating the angle between the mean  
 333       of the corrected DRM directions and the means of the CRM and lava directions, we con-  
 334       ducted common mean tests at each *f* factor (McFadden and McElhinny (1990); Fig. 5).  
 335       In each iteration, the *f* factor is deemed plausible if the null hypothesis that the two pop-  
 336       ulations share a common mean cannot be rejected. An *f* factor of 0.65 minimizes the  
 337       angle between the DRM and the volcanic directions ( $3.6^\circ$  angular difference) with the  
 338       populations having statistically indistinguishable populations (i.e. passing a common mean  
 339       test) between *f* factors of 0.75 and 0.56 (Fig. 5D). An *f* factor of 0.61 minimizes the an-  
 340       gle between the DRM and CRM ( $0.01^\circ$  angular difference) with statistically indistin-  
 341       guishable directions between 0.67 and 0.55 (Fig. 5C). These empirical *f* factors are similar  
 342       (Fig. 5E) with the uncertainty of the *f* factor determined through the DRM to CRM  
 343       comparison being smaller due to the higher number of vectors in the CRM population  
 344       ( $n=167$ ) than in the volcanics population ( $n=28$ ).

345       As an additional analysis, we grouped the specimens by grain size and compared  
 346       the specimen DRM directions to the volcanic directions. This analysis revealed claystone/siltstone  
 347       to have been shallowed the most ( $f = 0.56_{0.47}^{0.67}$ ), followed by the very fine-grained sand-

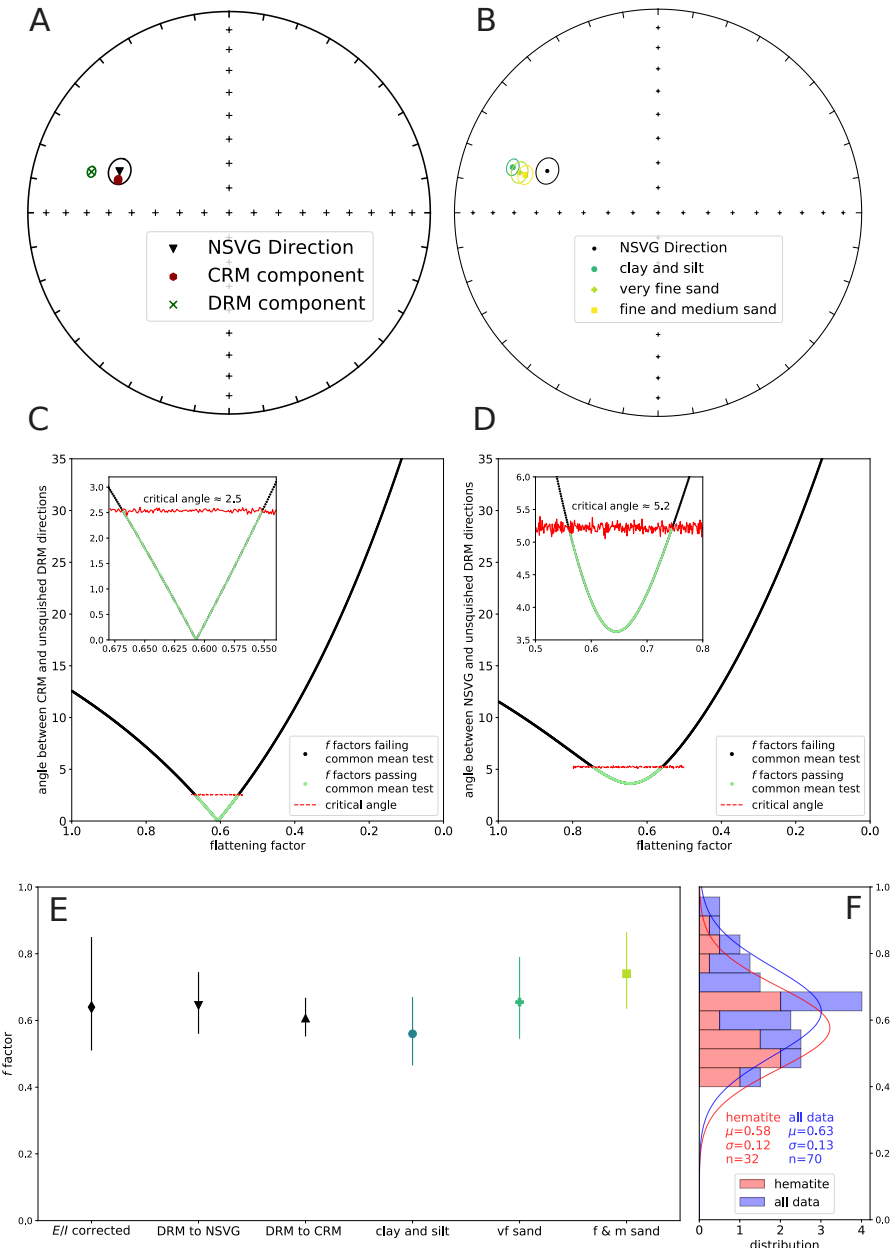


Figure 5: (A) Equal area plot comparing mean directions of Cut Face Creek Sandstone CRM and DRM magnetizations with that of the upper northeast sequence of the North Shore Volcanic Group (NSVG; Swanson-Hysell et al. (2019)). The mean CRM direction is indistinguishable from the volcanic direction while the DRM is shallowed relative to both. (B) Equal area plot comparing DRM directions of specimens grouped by grain size. Finer grain sizes have experienced more inclination shallowing. (C, D) Flattening factor estimates determined by progressively unflattening DRM directions and performing common mean tests between the DRM directions corrected by a given  $f$  factor and the CRM directions (in C) and the volcanics directions (in D). Green points are those that resulted in a statistically indistinguishable common mean (McFadden & McElhinny, 1990). The  $f$  factor resulting in the smallest angles and these common mean  $f$  factor test ranges for both DRM to NSVG volcanics and DRM to CRM are shown in (E) along with the  $f$  factor estimated using the  $E/I$  method and its associated 95% confidence bounds (Fig. 6). Also shown are the  $f$  factors and ranges for the DRM directions grouped by grain size compared to the NSVG directions. The stacked histogram in (F) summarizes compiled  $f$  factors for hematite-bearing sedimentary rocks as well as magnetite/mixed detrital magnetic mineralogy on the same axis as the estimates from this study in (E). A normal distribution fit to the  $f$  factors for hematite-bearing rocks has a mean of 0.58 with  $1\sigma$  of 0.12. A normal distribution fit to magnetite and hematite data has a mean of 0.63 with  $1\sigma$  of 0.13.

348 stones ( $f = 0.66_{0.55}^{0.79}$ ), with the inclinations of specimens of medium- to fine-grained sand-  
 349 stone being the least shallowed ( $f = 0.74_{0.64}^{0.87}$ ) (Fig. 5B,E).

### 350 4.3 Elongation/inclination flattening assessment

351 Applying the statistical  $E/I$  method to estimate the extent of inclination shallow-  
 352 ing yielded an  $f$  factor of 0.64 with a 95% confidence range of 0.85 to 0.51 (Fig. 6). This  
 353 uncertainty range is determined through 5,000 bootstrap resamples. The  $f$  factor esti-  
 354 mate of  $0.64_{0.51}^{0.85}$  obtained using the  $E/I$  method is very similar to that obtained empir-  
 355 ically through the comparison of the DRM to the volcanics ( $f = 0.65_{0.56}^{0.75}$ ) and the DRM  
 356 to the CRM ( $f = 0.61_{0.55}^{0.67}$ ) albeit with large associated uncertainty.

## 357 5 Discussion

### 358 5.1 Inclination shallowing in hematite-bearing sedimentary rocks

359 As has been long demonstrated in experimental and field studies (e.g. Tauxe & Kent,  
 360 1984; Lovlie & Torsvik, 1984), our study found that the remanence held by detrital hematite  
 361 was shallowed with respect to the field in which it was acquired. In contrast, the rema-  
 362 nence held by pigmentary hematite recovered the expected direction. The rapid accu-  
 363 mulation of subsequent lava flows within the North Shore Volcanic Group may have ac-  
 364 celerated the chemical transformation to pigmentary hematite of precursor iron oxide  
 365 phases such as ferrihydrite such that it occurred soon (<1 Myr) after deposition. In this  
 366 case, it is both interesting and useful that the CRM held by the pigmentary hematite  
 367 returns the expected direction. However, since it is inherently a secondary phase that  
 368 could be acquired on varied timescales, we caution against this result being broadly ex-  
 369 trapulated to other formations. As was found in the study of siltstone intraclasts by Swanson-  
 370 Hysell et al. (2019), high-resolution thermal demagnetization steps are necessary to iso-  
 371 late the DRM from the CRM. Isolating DRM held by detrital hematite is quite impor-  
 372 tant if one is then applying an inclination flattening correction given that the CRM of  
 373 pigmentary hematite is not expected to be flattened as shown in this study.

374 The  $f$  factors determined in this study of  $f = 0.65_{0.56}^{0.75}$  for the comparison of the  
 375 DRM to the volcanics,  $f = 0.61_{0.55}^{0.67}$  for the comparison of the DRM to the CRM, and  
 376  $0.64_{0.51}^{0.85}$  through the  $E/I$  method are all similar to one another (Fig. 5E). In addition,  
 377 they overlap with compiled  $f$  factors in the literature for hematite-bearing sedimentary

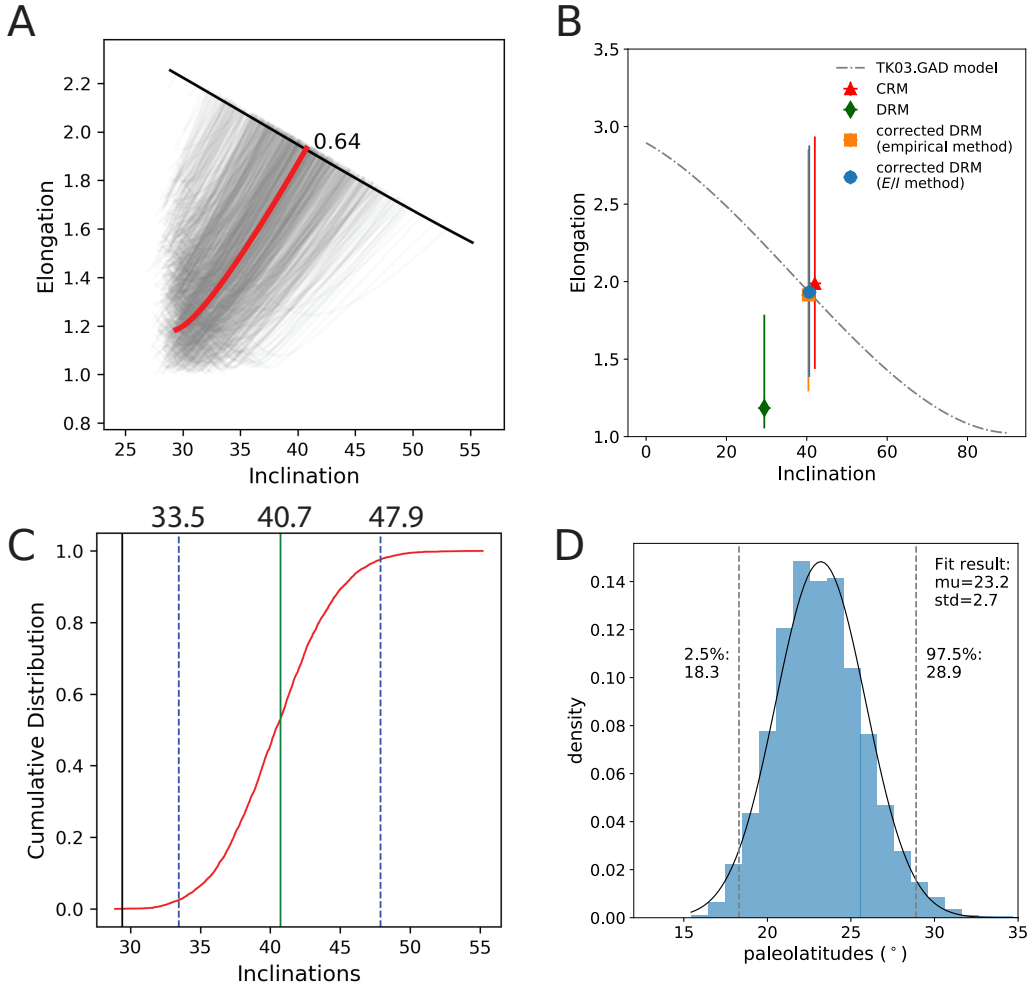


Figure 6: Results of the estimated amount of inclination shallowing of the detrital remanent magnetization of the Cut Face Creek sandstone using the elongation/inclination method (Tauxe & Kent, 2004). (A) The  $E/I$  method results in an estimated flattening factor of  $f=0.64$  (red curve) based on where elongation/inclination intersects that predicted by the TK03 paleosecular variation model (black curve). The grey lines show the analysis applied to 5,000 bootstrap resamples of the DRM directions of the Cut Face Creek Sandstone which provide an estimate of the uncertainty associated with the  $f$  factor estimate. B) The distribution of the CRM vectors (red triangle) as well as those for the DRM corrected with  $f=0.65$  (value that minimize the angle between the mean of the corrected DRM and the mean pole of the NSVG lava flows; orange square) have  $E/I$  values that are very close to that predicted by TK03.GAD. The DRM vectors corrected by the  $E/I$  method (blue circle) are directly on the TK03.GAD curve by definition of the method. C) The cumulative distribution of all plausible inclinations based on the  $E/I$  bootstrap results. D) The distribution of the paleolatitudes implied from the inclinations that result from the  $E/I$  method bootstrap resamples. The 95% confidence range spans a range of paleolatitudes that needs to be incorporated into the uncertainty on the resulting paleomagnetic pole.

378 rocks (Fig. 5F). One approach that has been taken in the literature is to assume an  $f$   
 379 factor of 0.6 and apply that to sedimentary poles for which no study specific factor was  
 380 determined (Domeier et al., 2012; Torsvik et al., 2012). This assumed value was informed

through a compilation of  $f$  factors developed using anisotropy approaches and the  $E/I$  method that was presented in Bilardello and Kodama (2010c). The  $f$  factor determined empirically for the Cut Face Creek Sandstone in this study is quite close to the assumed value of 0.6 applied to sedimentary paleomagnetic data by (Torsvik et al., 2012). However, numerous studies (e.g. Bilardello and Kodama (2010c) and Ding et al. (2015)) have cautioned against applying an assumed  $f$  factor and the variability in  $f$  factors between formations and within individual formations continues to be highlighted as inconsistent with a single value (e.g. Vaes et al., 2021). Our data corroborate this perspective as they reveal a relationship where the finer grained clay and siltstone lithologies are more flattened than the sandstone lithologies highlighting the variability of flattening in clastic sedimentary rocks as discussed in more detail below (Fig. 5).

## 5.2 Implications for applying the TK03 model and the $E/I$ method in deep time

The TK03 model for paleosecular variation, and therefore the target inclination-elongation curve that is used in the  $E/I$  method, was developed to match the variation of scatter within a compilation of lava flows for the past 5 Myr (McElhinny & McFadden, 1997; Tauxe & Kent, 2004). It remains an open question whether this model is representative of the field at times further back in Earth history. There is support that comes from compilations of data from large igneous provinces over the Phanerozoic Era, and back to the 1.1 Ga Midcontinent Rift, that yield inclination-elongation relationships consistent with that predicted by the model (Tauxe et al., 2008; Tauxe & Kodama, 2009). Additionally, comparisons between sedimentary inclinations corrected through the  $E/I$  method and coeval volcanics have been shown to yield consistent results in multiple studies including ca. 200 Ma (Kent & Olsen, 2008) and ca. 50 Ma (Vaes et al., 2021).

In our study, the close correspondence of the  $f$  factor determined through the  $E/I$  method and the empirical approach (Fig. 5E) supports the application of  $E/I$  at this time in the late Mesoproterozoic Era (the Stenian Period). A caveat to this conclusion is that there is large uncertainty on the  $f$  factor coming out of the bootstrap analysis as is typical when applying the  $E/I$  method to paleomagnetic data sets which limits the precision of the comparison. These uncertainties arise from the the reality that the shape of a distribution is more uncertain and prone to variability through bootstrap resampling than the mean of a distribution.

Another way to evaluate the applicability of the TK03 model in the late Mesoproterozoic is to consider the shape of the distribution of CRM directions (Fig. 6). These directions represent unflattened magnetization acquired as pigmentary hematite was growing within the sediment following deposition (likely from precursor ferric oxide phases). The relationship of the elongation and the unflattened inclination recorded by the pigmentary hematite corresponds closely with that of the TK03.GAD model (Fig. 6B). While there is appreciable uncertainty on the elongation estimate through this analysis (as represented in the bootstrap determined confidence bounds in Fig. 6B), it provides additional support for applying the TK03.GAD model in deep time.

### 5.3 Uncertainty in flattening factor estimates

Uncertainty is inherent to any method of estimating a flattening factor. Even in the case of an empirical flattening analysis with comparison to well-constrained unflattened time-equivalent directions as in this study, the uncertainty on mean directions leads to a range of plausible  $f$  factors (as determined through the common mean tests shown in Fig. 5). This range is more dramatic when the  $E/I$  method is applied given the limitations in tightly constraining the shape of a distribution from a population of vectors at a number that is feasible to obtain through paleomagnetic study. Correcting the DRM directions by the  $f$  values of 0.85 and 0.51 at the bounds of the 95% confidence interval found through  $E/I$  analysis (Fig. 6) will result in two distinct direction distributions (i.e. they fail a common mean test) whose mean directions are  $13.3^\circ$  apart. Such an angular difference in directional space translates into a  $9.7^\circ$  difference in calculated pole positions for the Cut Face Creek Sandstone. This difference highlights that such uncertainty on inclination needs to be incorporated into mean paleomagnetic poles developed from sedimentary rocks.

In addition to data analysis challenges which lead to inescapable uncertainty, there is also the reality that a sedimentary unit will have varying flattening factors in different horizons. Variability in ferromagnetic mineral assemblages, sedimentary grain size, and depositional processes—all of which are expected within a sedimentary formation—will impact flattening. The variability in inclination shallowing as a function of grain size has been shown in redeposition experiments such as those conducted by Tan et al. (2002) on disaggregated red beds. Their finding that deposits of finer grain size are more prone to inclination shallowing is consistent with our finding of shallower inclination in siltstone

445 than very fine sandstone which in turn is more shallowed than fine to medium sandstone  
 446 (Fig. 5B).

447 Despite expected variability in flattening factors within a single sedimentary rock  
 448 unit and inherent uncertainty in methods of determining  $f$  factors, studies typically use  
 449 a single  $f$  factor to correct for inclination shallowing. This approach holds true both in  
 450 studies that assume a single  $f$  factor (e.g. 0.6 applied to all sedimentary poles; Torsvik  
 451 et al. (2012)) as well as in studies that develop estimates through anisotropy approaches  
 452 or the  $E/I$  method both of which have associated uncertainty. In the case of the  $E/I$   
 453 method, researchers often consider the resulting  $f$  factor but do not incorporate the as-  
 454 sociated bootstrap uncertainty bounds when interpreting the data and developing as-  
 455 sociated paleomagnetic poles.

456 **5.4 Better representing inclination shallowing uncertainties in sedimen-**  
 457 **tary paleomagnetic poles**

458 Given that there is uncertainty in  $f$  factor regardless of method, this uncertainty  
 459 needs to be incorporated into the uncertainty on the mean pole position developed from  
 460 detrital remanent magnetization in sedimentary rocks. While paleomagnetic poles are  
 461 typically represented by circularly symmetric Fisher distributions, uncertainty in  $f$  fac-  
 462 tor will increase uncertainty in the direction between an unflattened paleomagnetic pole  
 463 and the study site such that the spherical uncertainty region is elliptical.

464 A strength of the  $E/I$  method is that the bootstrap approach to determine uncer-  
 465 tainty returns an ensemble of  $f$  factors that represents the uncertainty on the inclina-  
 466 tion correction. In Figure 6D, we show the distribution of paleolatitudes that results from  
 467 applying these  $f$  factors to variably correct the shallowed Cut Face Creek Sandstone DRM.  
 468 The resulting paleolatitude distribution can be approximated by a normal distribution  
 469 (mean=23.2°N; one standard deviation=2.7°; Fig. 6D). A Kent distribution implements  
 470 a bivariate normal distribution on a sphere which can therefore represent increased un-  
 471 certainty in the colatitude direction (the conjugate of paleolatitude) between the study  
 472 site and the paleomagnetic pole. The distribution shown in Fig. 6D has a heavy tail given  
 473 the transformation of directions to pole space such that representation with a normal  
 474 distribution is an approximation. However this is a useful approximation, as the Kent

475 distribution provides a succinct way to summarize the uncertainties associated with sed-  
 476 imentary paleomagnetic poles that include  $f$  factor uncertainty.

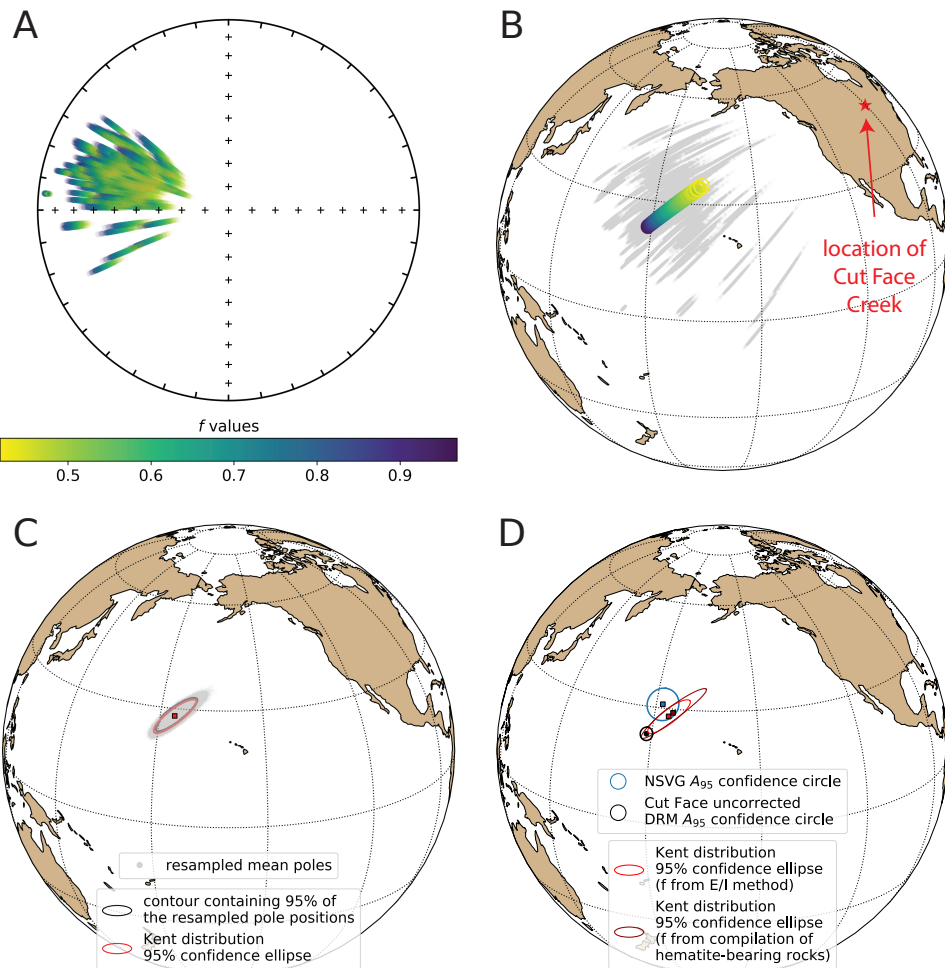


Figure 7: A new method for incorporating inclination shallowing uncertainty into sedimentary paleomagnetic poles. With each of the 5,000  $f$  values determined from the  $E/I$  method bootstrap resampling routine (Tauxe & Kent, 2004), we corrected all Cut Face Creek Sandstone DRM directions (shown colored by  $f$  factor in (A) and calculated their associated virtual geomagnetic pole positions (grey points in B). Mean pole positions with associated  $A_{95}$  calculated with Fisher statistics are shown in (B) also color-coded by the  $f$  factor that leads to that pole. To characterize the distribution shape, we Monte-Carlo resampled 100 random inclination-corrected mean pole positions from the angular standard deviation ( $\theta_{95}$ ) of the Fisher mean pole associated with each  $f$  value. The total 500,000 Monte-Carlo resampled results on the mean pole positions are shown as grey points in (C) along with the contour that encapsulates 95% of the resampled mean poles (in black). Also shown is the 95% confidence ellipse of the Kent distribution (red ellipse) which closely matches the 95% contour indicating that it is an effective summary of the distribution. The Kent distribution confidence ellipse for the Cut Face Creek pole that includes the  $f$  factor uncertainty resulting from the  $E/I$  method is shown in comparison with the North Shore Volcanic Group (NSVG) Fisher mean pole position in (D). Also, shown is the Kent distribution that results from applying the same approach with bootstrap resampled  $f$  factors taken from the compilation of published values. This approach could be applied to estimate the uncertainty of published sedimentary poles where  $E/I$  analysis is not possible.

To determine this uncertainty, we took all of the  $f$  factors from the  $E/I$  analysis (with 5,000 bootstrap resamples) and applied them to the DRM directions (Fig. 7A). Note that this can alternatively be done with a distribution of  $f$  factors associated with anisotropy uncertainty or from a compilation as discussed further below. For each  $f$  factor, we converted the directions to virtual geomagnetic poles (VGPs; grey in Fig. 7B) and calculated the mean paleomagnetic pole at each  $f$  factor as a Fisher mean (colored by  $f$  factor in Fig. 7B). What would typically be done with a single  $f$  factor (either calculated or assumed) is to take a single one of these poles as the resulting pole and report its Fisher mean which would underestimate uncertainty along the great circle between the pole and the study locality. Instead, we have an ensemble of possible poles associated with the ensemble of  $f$  factors. From these poles, we drew 100 random pole mean positions from each of the Fisher-distributed mean poles (grey poles in Fig. 7C). These resampled poles represent 500,000 possible mean pole positions and their elliptical distribution can be seen with the contour that contains 95% of the resampled mean pole positions (black curve in Fig. 7C). A Kent distribution calculated from these resampled mean poles that incorporates the flattening uncertainty is shown in red in Figure 7C and is very similar to the 95% contour. Kent distributions can be reported as the mean direction ( $\gamma_1$ ), the major axis ( $\gamma_2$ ) with a 95% semi-angle ( $\zeta_{95}$ ), and the minor axis ( $\gamma_3$ ) with a 95% semi-angle confidence angle ( $\eta_{95}$ ). The ellipse has its major axis along the great circle between  $\gamma_1$  and  $\gamma_2$  with its minor axis along the great circle between  $\gamma_1$  and  $\gamma_3$ . The Kent mean ellipse for the Cut Face Creek Sandstone incorporating flattening uncertainty from the  $E/I$  method has a mean of Plon=184.4°E, Plat = 28.1°N, a major axis of  $\gamma_2=[297.9^{\circ}\text{E}, 36.7^{\circ}\text{N}]$  with a semi-angle of  $\zeta_{95}=6.7^{\circ}$  and a minor axis of  $\gamma_3=[67.3^{\circ}\text{E}, 40.4^{\circ}\text{N}]$  with a semi-angle of  $\eta_{95}=1.8^{\circ}$ . The inclination corrected DRM Kent mean pole overlaps with the Fisher mean pole for the volcanics (Fig. 7).

For published datasets without estimates of inclination shallowing, one approach to incorporate the uncertainty associated with inclination shallowing is to use  $f$  factors from a compilation in contrast to assuming a single value (Bilardello & Kodama, 2008, 2009). Building on the compilations of Bilardello (2016) and Vaes et al. (2021), we compiled  $f$  factors from both anisotropy and  $E/I$  methods from clastic sedimentary rocks (Table S1). This compilation is summarized in the histogram in Figure 5F and Figure S1. The compilation reveals similar means and distributions between detrital magnetic mineralogies with slightly lower  $f$  values for hematite (Fig. 5F and Fig. S1). If an en-

Table 1: Kent mean paleomagnetic poles for the Cut Face Creek Sandstone

pole	mean pole	major axis	major axis	minor axis	minor axis
	position	95% confidence		95% confidence	
	(Plon/Plat)	angle	angle		
	$\gamma_1$	$\gamma_2$	$\zeta_{95}$	$\gamma_2$	$\eta_{95}$
Cut Face <i>E/I</i>	184.4°E /	297.9°E /	6.7°	67.3°E /	1.8°
corrected	28.1°N	36.7°N		40.4°N	
Cut Face compilation	185.7°E /	299.8°E /	10.8°	67.6°E /	1.7°
corrected	29.3°N	36.0°N		40.1°N	

Notes: The Fisher mean of the Cutface Creek paleomagnetic pole without an inclination  
shallowing correction is Plon=178.5, Plat=23.0, A<sub>95</sub>=1.7; the values associated with the  
compilation correction can slightly change with different bootstrap resampling runs given  
the relatively low number of *f* factors in the compilation.

semble of *f* factors resulting from the EI method is not available for a sedimentary paleomagnetic pole, these compiled *f* factors could be used to estimate the uncertainty associated with inclination shallowing and develop a Kent distribution pole. To do so, we follow the same approach described above with the modification of using *f* factors that are drawn from bootstrap resampling from the compilation. As is visualized in Figure 7D, the resulting uncertainty ellipse is larger than that when *f* factors come from the *E/I* analysis given that our knowledge of the inclination shallowing is less informed and taken from all estimated *f* factors. The Kent means and associated statistics resulting from applying the *E/I* correction and the compilation-based correction to the Cut Face Creek Sandstone are summarized in Table 1. Applying this method to synthetic and other sedimentary datasets yields similarly reasonable results as shown in the archived Jupyter notebooks accompanying this work.

Incorporating inclination shallowing uncertainty into the presentation of mean paleomagnetic poles has several advantages. It more completely communicates the uncer-

tainty associated with paleomagnetic poles developed from detrital remanent magnetization. Fisher mean paleomagnetic poles developed from sedimentary data often have small circular  $A_{95}$  confidence ellipses due to large numbers of samples in the mean. However, these small  $A_{95}$  uncertainty angles overestimate the confidence on the known position—particularly the co-latitude. Representing the uncertainty has the potential to reconcile disparate poles and address paleogeographic puzzles. Being able to approximate the mean pole position as a Kent distribution enables the mean pole and the uncertainty to be succinctly communicated. Additionally, the Kent distribution can be incorporated into frameworks such that probabilistic inversion or parametric Monte Carlo resampling can enable development of future apparent polar wander paths that incorporate uncertainty.

## 534 6 Conclusion

The Cut Face Creek Sandstone provides a 1.1-billion-year-old natural laboratory where the paleomagnetic pole position expected to have been recorded by the red beds can be tightly constrained by the lava flows that bracket it such that the amount of inclination shallowing of the sediments can be empirically determined. The statistical  $E/I$  method (Tauxe & Kent, 2004) yields an estimated range of  $f$  values for the hematite detrital remanent magnetization that agree with those derived empirically, but with larger uncertainties. Given that all methods have non-negligible uncertainties associated with determining the flattening factor, they should be recognized and incorporated into paleomagnetic syntheses. Incorporating uncertainty associated with inclination flattening leads to increased uncertainty in pole position between the unflattened pole position and the study site. We present a method that takes a range of unflattening factors and uses it to develop a mean pole and uncertainty ellipse that can be approximated as a Kent distribution. This method can be applied to datasets where  $f$  factors have been determined through  $E/I$  analysis as well as to datasets without such determination in which case the range of  $f$  factors can be taken from a literature compilation. Incorporating inclination shallowing uncertainty better represents our knowledge of ancient paleomagnetic pole positions thereby advancing paleogeographic reconstructions.

## 552 Acknowledgments

553 Support for this research came from NSF grant EAR-1847277 to Nicholas Swanson-Hysell  
 554 and an UC Berkeley Summer Undergraduate Research Fellowship awarded to James Pierce.

555 Lisa Tauxe provided inspiration and feedback on the approach taken in this study. Mar-  
556 garet Avery provided feedback on an earlier draft of the manuscript. Sarah Swanson-  
557 Hysell and Madeline Swanson-Hysell assisted with fieldwork. Dario Bilardello provided  
558 a compilation of  $f$  factors associated with Bilardello (2016) that he updated to include  
559 more recent data for the talk “The Anisotropy Correction for Inclination Shallowing”  
560 presented at the 2021 Institute for Rock Magnetism Conference. Paleomagnetic data as-  
561 sociated with this study are available within the MagIC database (<https://earthref.org/MagIC/19603/789b4868-fb73-4315-af37-81f599cacc4a>; UPDATE WHEN DOI  
562 IS GENERATED) and all data are within a Github repository associated with this work  
563 ([https://github.com/Swanson-Hysell-Group/Inclination\\_Shallowing](https://github.com/Swanson-Hysell-Group/Inclination_Shallowing)) that is also  
564 archived on Zenodo (<https://doi.org/XXX>; ZENODO RELEASE WILL BE MADE  
565 FROM GITHUB REPOSITORY UPON ACCEPTANCE). This repository also contains  
566 Python code that implements all of the calculations, visualizations and statistical tests  
567 discussed herein. We added to the Pmagpy Python package (Tauxe et al., 2016) a new  
568 function named *find\_ei\_kent* that finds the estimated range of plausible inclination shal-  
569 lowing factors for a set of sedimentary paleomagnetic directions using the  $E/I$  method  
570 and returns the associated Kent distribution that includes the uncertainty estimates from  
571 the  $E/I$  method to estimate the 95% confidence ellipse for a sedimentary paleomagnetic  
572 pole.  
573

574      **References**

- 575      Anson, G. L., & Kodama, K. P. (1987). Compaction-induced inclination shallowing  
 576      of the post-depositional remanent magnetization in a synthetic sediment. *Geophysical Journal International*, 88(3), 673–692.
- 578      Bilardello, D. (2015). Isolating the anisotropy of the characteristic remanence-  
 579      carrying hematite grains: a first multispecimen approach. *Geophysical Journal  
 580      International*, 202(2), 695–712. doi: 10.1093/gji/ggv171
- 581      Bilardello, D. (2016). The do's and don'ts of inclination shallowing corrections. *The  
 582      IRM Quarterly*, 26(3), 12.
- 583      Bilardello, D., Callebert, W. C., & Davis, J. R. (2018). Evidence for widespread  
 584      remagnetizations in South America, case study of the Itararé Group rocks  
 585      from the state of São Paulo, Brazil. *Frontiers in Earth Science*, 6. doi:  
 586      10.3389/feart.2018.00182
- 587      Bilardello, D., & Kodama, K. (2008). Poster: A simplified red bed inclination cor-  
 588      rection: A case study from the permian esterel rocks of france. In *American  
 589      Geophysical Union* (Vol. San Francisco, p. abstract id. GP51A-0733).
- 590      Bilardello, D., & Kodama, K. (2009). Poster: Magnetic fabric and inclination shal-  
 591      lowing studies: depositional and post-depositional processes in hematite- and  
 592      magnetite-bearing rocks. In *American Geophysical Union* (Vol. San Francisco,  
 593      p. abstract id. GP43A-0841).
- 594      Bilardello, D., & Kodama, K. P. (2010a). A new inclination shallowing correction of  
 595      the Mauch Chunk Formation of Pennsylvania, based on high-field AIR results:  
 596      Implications for the Carboniferous North American APW path and Pangea  
 597      reconstructions. *Earth and Planetary Science Letters*, 299(1-2), 218–227. doi:  
 598      10.1016/j.epsl.2010.09.002
- 599      Bilardello, D., & Kodama, K. P. (2010b). Palaeomagnetism and magnetic anisotropy  
 600      of Carboniferous red beds from the Maritime Provinces of Canada: evidence  
 601      for shallow palaeomagnetic inclinations and implications for North American  
 602      apparent polar wander. *Geophysical Journal International*, 180(3), 1013–1029.  
 603      doi: 10.1111/j.1365-246X.2009.04457.x
- 604      Bilardello, D., & Kodama, K. P. (2010c). Rock magnetic evidence for inclination  
 605      shallowing in the early Carboniferous Deer Lake Group red beds of western  
 606      Newfoundland. *Geophysical Journal International*, 181(1), 275–289. doi:

- 607                   10.1111/j.1365-246X.2010.04537.x
- 608 Books, K. (1972). *Paleomagnetism of Some Lake Superior Keweenawan Rocks*. Geo-  
609                   logical Survey Professional Paper 760.
- 610 Butler, R. F. (1992). *Magnetic Domains to Geologic Terranes*. Blackwell Scientific  
611                   Publications.
- 612 Cant, D. J., & Walker, R. G. (1976). Development of a braided-fluvial facies model  
613                   for the Devonian Battery Point Sandstone, Québec. *Canadian Journal of*  
614                   *Earth Sciences*, 13(1), 102–119. doi: 10.1139/e76-010
- 615 Chen, W., Zhang, S., Ding, J., Zhang, J., Zhao, X., Zhu, L., ... Wu, H. (2017).  
616                   Combined paleomagnetic and geochronological study on Cretaceous strata of  
617                   the Qiangtang terrane, central Tibet. *Gondwana Research*, 41, 373–389. doi:  
618                   10.1016/j.gr.2015.07.004
- 619 Costa, E., Garces, M., López-Blanco, M., Beamud, E., Gómez-Paccard, M., & Lar-  
620                   rasoña, J. C. (2009). Closing and continentalization of the South Pyrenean  
621                   foreland basin (NE Spain): magnetochronological constraints. *Basin Research*.  
622                   doi: 10.1111/j.1365-2117.2009.00452.x
- 623 Dallanave, E., Kirscher, U., Hauck, J., Hesse, R., Bachtadse, V., & Wortmann, U. G.  
624                   (2018). Palaeomagnetic time and space constraints of the Early Cretaceous  
625                   Rhenodanubian Flysch zone (Eastern Alps). *Geophysical Journal Interna-*  
626                   *tional*, 213(3), 1804–1817. doi: 10.1093/gji/ggy077
- 627 Deenen, M. H. L., Langereis, C. G., van Hinsbergen, D. J. J., & Biggin, A. J.  
628                   (2011). Geomagnetic secular variation and the statistics of palaeomag-  
629                   netic directions. *Geophysical Journal International*. doi: 10.1111/  
630                   j.1365-246X.2011.05050.x
- 631 Ding, J., Zhang, S., Chen, W., Zhang, J., Yang, T., Jiang, G., ... Wu, H. (2015).  
632                   Paleomagnetism of the Oligocene Kangtuo Formation red beds (Central Ti-  
633                   bet): Inclination shallowing and tectonic implications. *Journal of Asian Earth*  
634                   *Sciences*, 104, 55–68. doi: 10.1016/j.jseas.2014.10.006
- 635 Domeier, M., Van der Voo, R., & Torsvik, T. H. (2012). Paleomagnetism and  
636                   Pangea: The road to reconciliation. *Tectonophysics*, 514-517, 14–43. doi:  
637                   10.1016/j.tecto.2011.10.021
- 638 Dupont-Nivet, G., Lippert, P. C., Hinsbergen, D. J. V., Meijers, M. J., & Kapp,  
639                   P. (2010). Palaeolatitude and age of the Indo-Asia collision: palaeomag-

- netic constraints. *Geophysical Journal International*, 182(3), 1189–1198. doi: 10.1111/j.1365-246x.2010.04697.x

Gallo, L. C., Tomezzoli, R. N., & Cristallini, E. O. (2017). A pure dipole analysis of the Gondwana apparent polar wander path: Paleogeographic implications in the evolution of Pangea. *Geochemistry, Geophysics, Geosystems*, 18(4), 1499–1519. doi: 10.1002/2016gc006692

Green, J. C. (1983). Geologic and geochemical evidence for the nature and development of the middle Proterozoic (Keweenawan) Midcontinent Rift of North America. *Tectonophysics*, 94(1), 413–437. doi: 10.1016/0040-1951(83)90027-6

Green, J. C., Boerboom, T. J., Schmidt, S. T., & Fitz, T. J. (2011). The North Shore Volcanic Group: Mesoproterozoic plateau volcanic rocks of the Midcontinent Rift system in northeastern Minnesota. *Archean to Anthropocene: Field Guides to the Geology of the Mid-Continent of North America: Geological Society of America Field Guide*, 24, 121–146.

Gutiérrez, L., Barrón, V., Andrés-Vergés, M., Serna, C. J., Veintemillas-Verdaguer, S., Morales, M. P., & Lázaro, F. J. (2016). Detailed magnetic monitoring of the enhanced magnetism of ferrihydrite along its progressive transformation into hematite. *Journal of Geophysical Research: Solid Earth*, 121(6), 4118–4129. doi: 10.1002/2016JB013016

Haldan, M. M., Langereis, C. G., Biggin, A. J., Dekkers, M. J., & Evans, M. E. (2009). A comparison of detailed equatorial red bed records of secular variation during the Permo-Carboniferous Reversed Superchron. *Geophysical Journal International*, 177(3), 834–848. doi: 10.1111/j.1365-246x.2009.04124.x

Huang, W., Dupont-Nivet, G., Lippert, P. C., van Hinsbergen, D. J. J., & Hallot, E. (2013). Inclination shallowing in Eocene Linzizong sedimentary rocks from Southern Tibet: correction, possible causes and implications for reconstructing the India–Asia collision. *Geophysical Journal International*, 194(3), 1390–1411. doi: 10.1093/gji/ggt188

Huang, W., van Hinsbergen, D. J., Maffione, M., Orme, D. A., Dupont-Nivet, G., Guilmette, C., ... Kapp, P. (2015). Lower Cretaceous Xigaze ophiolites formed in the Gangdese forearc: Evidence from paleomagnetism, sediment provenance, and stratigraphy. *Earth and Planetary Science Letters*, 415, 142–153. doi: 10.1016/j.epsl.2015.01.032

- 673 Jackson, M. J., Banerjee, S. K., Marvin, J. A., Lu, R., & Gruber, W. (1991). Detrital remanence, inclination Errors, and anhysteretic remanence anisotropy:  
674 Quantitative model and experimental results. *Geophysical Journal International*, 104(1), 95–103. doi: 10.1111/j.1365-246X.1991.tb02496.x
- 677 Jiang, Z., Liu, Q., Dekkers, M. J., Tauxe, L., Qin, H., Barrón, V., & Torrent, J.  
678 (2015). Acquisition of chemical remanent magnetization during experimental  
679 ferrihydrite–hematite conversion in Earth-like magnetic field—implications for  
680 paleomagnetic studies of red beds. *Earth and Planetary Science Letters*, 428,  
681 1–10. doi: 10.1016/j.epsl.2015.07.024
- 682 Jiang, Z., Liu, Q., Roberts, A. P., Barrón, V., Torrent, J., & Zhang, Q. (2018). A  
683 new model for transformation of ferrihydrite to hematite in soils and sedi-  
684 ments. *Geology*. doi: 10.1130/G45386.1
- 685 Jiang, Z., Liu, Q., Roberts, A. P., Dekkers, M. J., Barrón, V., Torrent, J., & Li, S.  
686 (2022). The magnetic and color reflectance properties of hematite: From Earth  
687 to Mars. *Reviews of Geophysics*, 60(1). doi: 10.1029/2020rg000698
- 688 Jirsa, M. A. (1984). Interflow Sedimentary Rocks in the Keweenawan North Shore  
689 Volcanic Group, Northeastern Minnesota. *Minnesota Geological Survey*, 28.
- 690 Kent, D. V., & Olsen, P. E. (2008). Early Jurassic magnetostratigraphy and pale-  
691 olatitudes from the Hartford continental rift basin (eastern North America):  
692 Testing for polarity bias and abrupt polar wander in association with the  
693 central Atlantic magmatic province. *Journal of Geophysical Research: Solid  
694 Earth*, 113(B6). doi: doi.org/10.1029/2007JB005407
- 695 Kent, D. V., & Tauxe, L. (2005). Corrected late triassic latitudes for continents ad-  
696 jacent to the north atlantic. *Science*, 307(5707), 240–244. doi: 10.1126/science  
697 .1105826
- 698 Kim, B., & Kodama, K. P. (2004). A compaction correction for the paleomagnetism  
699 of the Nanaimo Group sedimentary rocks: Implications for the Baja British  
700 Columbia hypothesis. *Journal of Geophysical Research: Solid Earth*, 109(B2).  
701 doi: 10.1029/2003jb002696
- 702 King, R. F. (1955). The remanent magnetism of artificially deposited sediments.  
703 *Geophysical Supplements to the Monthly Notices of the Royal Astronomical  
704 Society*, 7(3), 115–134. doi: 10.1111/j.1365-246X.1955.tb06558.x
- 705 Kirscher, U., Bilardello, D., Mikolaichuk, A., & Bachtadse, V. (2014). Correcting for

- 706 inclination shallowing of early Carboniferous sedimentary rocks from Kyrgyzstan—indication of stable subtropical position of the North Tianshan Zone in  
707 the mid-late Palaeozoic. *Geophysical Journal International*, 198(2), 1000–1015.  
708 doi: 10.1093/gji/ggu177
- 710 Kirschvink, J. L. (1980). The least-squares line and plane and the analysis of palaeo-  
711 magnetic data. *Geophysical Journal International*, 62(3), 699–718. doi: 10  
712 .1111/j.1365-246X.1980.tb02601.x
- 713 Kodama, K. P. (2009). Simplification of the anisotropy-based inclination cor-  
714 rection technique for magnetite- and haematite-bearing rocks: a case study  
715 for the Carboniferous Glenshaw and Mauch Chunk Formations, North  
716 America. *Geophysical Journal International*, 176(2), 467–477. doi:  
717 10.1111/j.1365-246x.2008.04013.x
- 718 Kodama, K. P. (2012). *Paleomagnetism of sedimentary rocks: process and interpre-  
719 tation*. Chichester, West Sussex ; Hoboken, NJ: John Wiley & Sons.
- 720 Kodama, K. P., & Davi, J. M. (1995). A compaction correction for the paleomag-  
721 netism of the Cretaceous Pigeon Point Formation of California. *Tectonics*,  
722 14(5), 1153–1164. doi: 10.1029/95tc01648
- 723 Krijgsman, W., & Tauxe, L. (2004). Shallow bias in Mediterranean paleomagnetic  
724 directions caused by inclination error. *Earth and Planetary Science Letters*,  
725 222(2), 685–695. doi: 10.1016/j.epsl.2004.03.007
- 726 Krijgsman, W., & Tauxe, L. (2006). E/I corrected paleolatitudes for the sedimen-  
727 tary rocks of the Baja British Columbia hypothesis. *Earth and Planetary Sci-  
728 ence Letters*, 242(1-2), 205–216. doi: 10.1016/j.epsl.2005.11.052
- 729 Lanci, L., Tohver, E., Wilson, A., & Flint, S. (2013). Upper Permian magnetic  
730 stratigraphy of the lower Beaufort Group, Karoo Basin. *Earth and Planetary  
731 Science Letters*, 375, 123–134. doi: 10.1016/j.epsl.2013.05.017
- 732 Li, S., Li, Y., Tan, X., Wang, C., Han, Z., Xiao, S., ... Zhang, J. (2022). New pale-  
733 omagnetic results of the Upper Cretaceous to Lower Eocene sedimentary rocks  
734 from the Xigaze forearc basin and their tectonic implications. *Tectonophysics*,  
735 837, 229433. doi: 10.1016/j.tecto.2022.229433
- 736 Li, Y., Kodama, K., & Smith, D. (2001). A compaction-corrected inclination for the  
737 Middle Cretaceous Valle Group in Vizcaino Terrane, Baja California, Mexico:  
738 preliminary results. In *Agu fall meeting abstracts* (pp. GP41A–0256).

- 739 Lovlie, R., & Torsvik, T. (1984). Magnetic remanence and fabric properties of  
740 laboratory-deposited hematite-bearing red sandstone. *Geophys. Res. Lett.*,  
741 11(3), 221–224. doi: 10.1029/GL011i003p00221
- 742 Lu, H. M., & Meng, X. K. (2010). Morin temperature and Néel temperature of  
743 hematite nanocrystals. *The Journal of Physical Chemistry C*, 114(49), 21291–  
744 21295. doi: 10.1021/jp108703b
- 745 McElhinny, M. W., & McFadden, P. L. (1997). Palaeosecular variation over the  
746 past 5 Myr based on a new generalized database. *Geophysical Journal Interna-*  
747 *tional*, 131(2), 240–252. doi: 10.1111/j.1365-246X.1997.tb01219.x
- 748 McFadden, P. L., & McElhinny, M. W. (1990). Classification of the reversal test in  
749 palaeomagnetism. *Geophysical Journal International*, 103(3), 725–729. doi: 10  
750 .1111/j.1365-246X.1990.tb05683.x
- 751 Meijers, M. J. M., Kaymakci, N., van Hinsbergen, D. J. J., Langereis, C. G.,  
752 Stephenson, R. A., & Hippolyte, J.-C. (2010). Late Cretaceous to Pale-  
753 ocene oroclinal bending in the central Pontides (Turkey). *Tectonics*, 29(4).  
754 doi: 10.1029/2009tc002620
- 755 Meng, J., Coe, R. S., Wang, C., Gilder, S. A., Zhao, X., Liu, H., ... Li, S. (2017).  
756 Reduced convergence within the Tibetan Plateau by 26 Ma? *Geophysical Re-*  
757 *search Letters*, 44(13), 6624–6632. doi: 10.1002/2017gl074219
- 758 Milanese, F., Rapalini, A., Slotnick, S. P., Tobin, T. S., Kirschvink, J., & Olivero,  
759 E. (2019). Late Cretaceous paleogeography of the Antarctic Peninsula: New  
760 paleomagnetic pole from the James Ross Basin. *Journal of South American  
761 Earth Sciences*, 91, 131–143. doi: 10.1016/j.jsames.2019.01.012
- 762 Miller, J., James D., Green, J. C., Severson, M. J., Chandler, V. W., & Peterson,  
763 D. M. (2001). *M-119 Geologic map of the Duluth Complex and related rocks,  
764 northeastern Minnesota* (Tech. Rep.). Minnesota Geological Survey.
- 765 Mitchell, R., & Sheldon, N. (2009). Weathering and paleosol formation in the 1.1 Ga  
766 Keweenawan Rift. *Precambrian Research*, 168(3-4), 271–283. doi: 10.1016/j  
767 .precamres.2008.09.013
- 768 Sun, W. W., & Kodama, K. P. (1992). Magnetic anisotropy, scanning electron mi-  
769 croscopy, and X ray pole figure goniometry study of inclination shallowing in a  
770 compacting clay-rich sediment. *Journal of Geophysical Research: Solid Earth*,  
771 97(B13), 19599–19615. doi: 10.1029/92JB01589

- 772 Swanson-Hysell, N. L., Hoaglund, S. A., Crowley, J. L., Schmitz, M. D., Zhang,  
773 Y., & Miller, J. D. (2021). Rapid emplacement of massive Duluth Com-  
774 plex intrusions within the North American Midcontinent Rift. *Geology*. doi:  
775 10.1130/G47873.1
- 776 Swanson-Hysell, N. L., Ramezani, J., Fairchild, L. M., & Rose, I. R. (2019). Failed  
777 rifting and fast drifting: Midcontinent Rift development, Laurentia's rapid mo-  
778 tion and the driver of Grenvillian orogenesis. *GSA Bulletin*, 131(5-6), 913–940.  
779 doi: 10.1130/B31944.1
- 780 Swanson-Hysell, N. L., Fairchild, L. M., & Slotznick, S. P. (2019). Primary  
781 and secondary red bed magnetization constrained by fluvial intraclasts.  
782 *Journal of Geophysical Research: Solid Earth*, 124(5), 4276–4289. doi:  
783 10.1029/2018JB017067
- 784 Tan, X., Gilder, S., Kodama, K. P., Jiang, W., Han, Y., Zhang, H., ... Zhou, D.  
785 (2010). New paleomagnetic results from the Lhasa block: Revised estima-  
786 tion of latitudinal shortening across Tibet and implications for dating the  
787 India–Asia collision. *Earth and Planetary Science Letters*, 293(3-4), 396–404.  
788 doi: 10.1016/j.epsl.2010.03.013
- 789 Tan, X., & Kodama, K. P. (1998). Compaction-corrected inclinations from southern  
790 California Cretaceous marine sedimentary rocks indicate no paleolatitudinal  
791 offset for the Peninsular Ranges terrane. *Journal of Geophysical Research:*  
792 *Solid Earth*, 103(B11), 27169–27192. doi: 10.1029/98jb02343
- 793 Tan, X., Kodama, K. P., Chen, H., Fang, D., Sun, D., & Li, Y. (2003). Paleomag-  
794 netism and magnetic anisotropy of Cretaceous red beds from the Tarim basin,  
795 northwest China: Evidence for a rock magnetic cause of anomalously shallow  
796 paleomagnetic inclinations from central Asia. *Journal of Geophysical Research:*  
797 *Solid Earth*, 108(B2). doi: 10.1029/2001jb001608
- 798 Tan, X., Kodama, K. P., & Fang, D. (2002). Laboratory depositional and  
799 compaction-caused inclination errors carried by haematite and their im-  
800 plications in identifying inclination error of natural remanence in red  
801 beds. *Geophysical Journal International*, 151(2), 475–486. doi: 10.1046/  
802 j.1365-246X.2002.01794.x
- 803 Tauxe, L. (2005). Inclination flattening and the geocentric axial dipole hypothe-  
804 sis. *Earth and Planetary Science Letters*, 233(3-4), 247–261. doi: 10.1016/j

- 805 .epsl.2005.01.027
- 806 Tauxe, L., & Kent, D. V. (1984). Properties of a detrital remanence carried by  
807 haematite from study of modern river deposits and laboratory redeposition experiments.  
808 *Geophysical Journal International*, 76(3), 543–561. doi:  
809 10.1111/j.1365-246X.1984.tb01909.x
- 810 Tauxe, L., & Kent, D. V. (2004). A simplified statistical model for the geomagnetic  
811 field and the detection of shallow bias in paleomagnetic inclinations: was  
812 the ancient magnetic field dipolar? In *Geophysical Monograph Series* (pp.  
813 101–115). American Geophysical Union. doi: 10.1029/145GM08
- 814 Tauxe, L., Kent, D. V., & Opdyke, N. D. (1980). Magnetic components contributing  
815 to the NRM of Middle Siwalik red beds. *Earth and Planetary Science Letters*,  
816 47(2), 279–284. doi: 10.1016/0012-821X(80)90044-8
- 817 Tauxe, L., & Kodama, K. P. (2009). Paleosecular variation models for ancient times:  
818 Clues from Keweenawan lava flows. *Physics of the Earth and Planetary Interiors*,  
819 177(1), 31–45. doi: 10.1016/j.pepi.2009.07.006
- 820 Tauxe, L., Kodama, K. P., & Kent, D. V. (2008). Testing corrections for pa-  
821 leomagnetic inclination error in sedimentary rocks: A comparative ap-  
822 proach. *Physics of the Earth and Planetary Interiors*, 169(1), 152–165. doi:  
823 10.1016/j.pepi.2008.05.006
- 824 Tauxe, L., Shaar, R., Jonestrask, L., Swanson-Hysell, N. L., Minnett, R., Koppers,  
825 A. a. P., ... Fairchild, L. (2016). PmagPy: Software package for paleomagnetic  
826 data analysis and a bridge to the MagNETics Information Consortium (MagIC)  
827 Database. *Geochemistry, Geophysics, Geosystems*, 17(6), 2450–2463. doi:  
828 10.1002/2016GC006307
- 829 Tong, Y., Yang, Z., Mao, C., Pei, J., Pu, Z., & Xu, Y. (2017). Paleomagnetism of  
830 Eocene red-beds in the eastern part of the Qiangtang Terrane and its impli-  
831 cations for uplift and southward crustal extrusion in the southeastern edge of  
832 the Tibetan Plateau. *Earth and Planetary Science Letters*, 475, 1–14. doi:  
833 10.1016/j.epsl.2017.07.026
- 834 Tong, Y.-B., Yang, Z., Zheng, L.-D., Xu, Y.-L., Wang, H., Gao, L., & Hu, X.-  
835 Z. (2013). Internal crustal deformation in the northern part of Shan-Thai  
836 Block: New evidence from paleomagnetic results of Cretaceous and Paleogene  
837 redbeds. *Tectonophysics*, 608, 1138–1158. doi: 10.1016/j.tecto.2013.06.031

- 838 Torsvik, T. H., Van der Voo, R., Preeden, U., Mac Niocaill, C., Steinberger, B.,  
 839 Doubrovine, P. V., ... Cocks, L. R. M. (2012). Phanerozoic polar wander,  
 840 palaeogeography and dynamics. *Earth-Science Reviews*, 114(3), 325–368. doi:  
 841 10.1016/j.earscirev.2012.06.007
- 842 Vaes, B., Li, S., Langereis, C. G., & van Hinsbergen, D. J. J. (2021). Reliability  
 843 of palaeomagnetic poles from sedimentary rocks. *Geophysical Journal Interna-*  
 844 *tional*, 225(2), 1281–1303. doi: 10.1093/gji/ggab016
- 845 van Hinsbergen, D. J., Krijgsman, W., Langereis, C. G., Cornée, J.-J., Duermei-  
 846 jer, C. E., & van Vugt, N. (2007). Discrete Plio-Pleistocene phases of tilt-  
 847 ing and counterclockwise rotation in the southeastern Aegean arc (Rhodos,  
 848 Greece): early Pliocene formation of the south Aegean left-lateral strike-  
 849 slip system. *Journal of the Geological Society*, 164(6), 1133–1144. doi:  
 850 10.1144/0016-76492006-061
- 851 van Hinsbergen, D. J. J., Dekkers, M. J., & Koc, A. (2010). Testing Miocene re-  
 852 magnetization of Bey Dağları: Timing and amount of Neogene rotations in SW  
 853 Turkey. *Turkish Journal of Earth Sciences*, 19(2), 123–156.
- 854 van Hinsbergen, D. J. J., Lippert, P. C., Dupont-Nivet, G., McQuarrie, N.,  
 855 Doubrovine, P. V., Spakman, W., & Torsvik, T. H. (2012). Greater India  
 856 Basin hypothesis and a two-stage Cenozoic collision between India and Asia.  
 857 *Proceedings of the National Academy of Sciences*, 109(20), 7659–7664. doi:  
 858 10.1073/pnas.1117262109
- 859 van Toorenenburg, K. A., Donselaar, M. E., & Weltje, G. J. (2018). The life cycle  
 860 of crevasse splays as a key mechanism in the aggradation of alluvial ridges and  
 861 river avulsion. *Earth Surface Processes and Landforms*, 43(11), 2409–2420.  
 862 doi: 10.1002/esp.4404
- 863 Vaughn, J., Kodama, K. P., & Smith, D. P. (2005). Correction of inclination shal-  
 864 lowing and its tectonic implications: The Cretaceous Perforada Formation,  
 865 Baja California. *Earth and Planetary Science Letters*, 232(1-2), 71–82. doi:  
 866 10.1016/j.epsl.2004.11.026
- 867 Westerweel, J., Roperch, P., Licht, A., Dupont-Nivet, G., Win, Z., Poblete, F., ...  
 868 Aung, D. W. (2019). Burma Terrane part of the Trans-Tethyan arc during  
 869 collision with India according to palaeomagnetic data. *Nature Geoscience*,  
 870 12(10), 863–868. doi: 10.1038/s41561-019-0443-2

- 871 Yan, M., Van der Voo, R., Tauxe, L., Fang, X., & M Parés, J. (2005). Shallow bias  
872 in Neogene palaeomagnetic directions from the Guide Basin, NE Tibet, caused  
873 by inclination error. *Geophysical Journal International*, 163(3), 944–948. doi:  
874 10.1111/j.1365-246X.2005.02802.x
- 875 Zhang, Y., Huang, W., Huang, B., Hinsbergen, D. J. J., Yang, T., Dupont-Nivet,  
876 G., & Guo, Z. (2018). 53–43 Ma deformation of eastern Tibet revealed by  
877 three stages of tectonic rotation in the Gongjue Basin. *Journal of Geophysical  
878 Research: Solid Earth*, 123(5), 3320–3338. doi: 10.1002/2018jb015443
- 879 Zhang, Y., Swanson-Hysell, N. L., Schmitz, M. D., Miller, J. D., & Avery, M. S.  
880 (2021). Synchronous emplacement of the anorthosite xenolith-bearing Beaver  
881 River diabase and one of the largest lava flows on Earth. *Geochemistry, Geo-  
882 physics, Geosystems*, 22(10), e2021GC009909. doi: 10.1029/2021GC009909
- 883 Özdemir, , & Dunlop, D. J. (2014). Hysteresis and coercivity of hematite.  
884 *Journal of Geophysical Research: Solid Earth*, 119(4), 2582–2594. doi:  
885 10.1002/2013JB010739